Dyes and Pigments 93 (2012) 1408–1415

Contents lists available at SciVerse ScienceDirect

Dyes and Pigments

journal homepage: www.elsevier.com/locate/dyepig

Merocyanine dyes containing an isoxazolone nucleus: Synthesis, X-ray crystal structures, spectroscopic properties and DFT studies

Xiang-Han Zhang [a,*], Yong-Hua Zhan [a], Dan Chen [a], Fu Wang [a], Lan-Ying Wang [b,**]

[a] *Life Sciences Research Center, School of Life Sciences and Technology, Xidian University, Xi'an, Shaanxi 710071, PR China*
[b] *Key Laboratory of Synthetic and Natural Functional Molecule Chemistry (Ministry of Education), College of Chemistry and Materials Science, Northwest University, Xi'an, Shaanxi 710069, PR China*

ARTICLE INFO

Article history:
Received 3 August 2011
Received in revised form
26 September 2011
Accepted 5 October 2011
Available online 15 October 2011

Keywords:
Merocyanine dyes
X-ray diffraction
H-bond
Solvent effect
Vibrational spectroscopy
DFT calculations

ABSTRACT

Two merocyanine dyes, each with an isoxazolone nucleus, were synthesized and characterized by NMR, IR, UV–Vis spectroscopy, elemental analyses and single X-ray diffraction. Crystallographic data revealed that one dye crystallized in an orthorhombic system, Cmca space group, while the other dye crystallized in a monoclinic system, $P2_1/n$ space group. In the case of both dyes, the molecules adopted the most stable ketonic tautomeric form, and the crystal packing was stabilized by hydrogen bonds and π–π stacking interactions. The absorption spectra of the dyes in various solvents of different polarities were studied at room temperature. The equilibrium geometries, vibrational data and electronic spectra of the compounds were also investigated by the B3LYP method. Importantly, the predicted results fit to the experimental data, showing that this quantum chemical technology is an efficient approach to predict the properties of merocyanine dyes.

1. Introduction

Isoxazolone functional groups have attracted considerable attention for use in the design of biologically active molecules and advanced organic materials. Due to their excellent biological activities and unique pharmacophores, isoxazolone derivatives have been widely used as anti-androgens and inhibitors in the therapy of diverse diseases [1–5], as well as in herbicides for agriculture [6,7]. Furthermore, an isoxazolone nucleus is a good proaromatic acceptor, when linked to aromatic donors, for conjugated donor-acceptor (D–π–A) merocyanine dyes [8,9]. Because of their good molar extinction coefficients, tunable absorption spectra, and large first molecular hyperpolarizabilities (β), merocyanine dyes with an isoxazolone nucleus have been used for optical recording and nonlinear optical research [10].

In this paper, two merocyanine dyes, each with an isoxazolone nucleus, were synthesized. The X-ray crystal structures of the two dyes correlated with the IR spectra, specifically demonstrating the molecular conformations and intra- and intermolecular interactions. A number of details of the X-ray crystallography leading to the molecular conformation or intermolecular interactions of cyanine and merocyanine dyes remain useful and are a view to their practical application [11]. Interestingly, isoxazolone derivatives can exist in three tautomeric forms: the OH form, the C=O form and the NH form. A mixture of these is always obtained, but the ketonic forms are generally predominant [12]. Based on the X-ray crystal results in this study, theoretical chemistry, like density functional theory (DFT), is valuable [13–15] in validating the experimental data for the tautomerism of merocyanine with an isoxazolone nucleus.

In order to obtain greater insight into the multicolor of the dyes, we mainly focused on the effect of the solvent on the electronic absorption of the dyes by means of experimental and theoretical methods. The TDDFT level with vertical SCRF approach reproduced the solvatochromism of the dyes, which depended on the surrounding solvent molecules and a polarizable continuum. It has been shown that theoretical calculations on the chromophoric properties of organic dyes are indispensable tools for practical applications and should help in predicting and explaining the structure–property relationships of the dyes [16–19]. Therefore, resonance frequency calculations were carried out for preliminary studies of the IR spectra of the dyes. For experimental vibrational spectroscopy that lacks a direct relation between the spectra and

---

[*] Corresponding author. Tel.: +86 29 81891070; fax: +86 29 81891060.
[**] Corresponding author.

E-mail addresses: zhangxianghan@life.xidian.edu.cn (X.-H. Zhang), wanglany@nwu.edu.cn (L.-Y. Wang).

0143-7208/$ – see front matter © 2011 Elsevier Ltd. All rights reserved.
doi:10.1016/j.dyepig.2011.10.003

the structure, theoretical predictions of vibrational spectra are of practical value for the identification of known and unknown compounds [20–22]. Thus, theoretical predictions, preferably those used with DFT methods, are advantageous. In this work, we followed this approach, and the detailed results and discussion are elaborated in the following sections.

2. Experimental

2.1. Synthesis

The general route for the synthesis of dyes (**1**) and (**2**) is shown in Scheme 1. To a stirred mixture of hydroxylamine hydrochloride (4 mmol), pyridine (4 mmol) in EtOH (10 mL), ethyl acetoacetate (4 mmol) was added via a dropping funnel over a 30 min time span. Then, either 1H-indole-3-carbaldehyde (3.5 mmol) or 5-benzyloxy-1H-indole-3-carbaldehyde (3.5 mmol) was added, and the mixture was stirred under reflux for 2 h [23]. After cooling, the precipitated crude dyes were filtered and then washed thoroughly with ether and ethanol. The solid was purified by recrystallization using EtOH–MeOH, resulting in pure dyes (**1**) and (**2**) (yields of 67% and 60%, respectively). Single crystals of dyes (**1**) and (**2**) were grown from an EtOH–MeOH mixture (1:2) or EtOH–acetone mixture (1:1), respectively, for X-ray diffraction experiments.

Dye (**1**) (4-[(1*H*-indole-3-yl)-methylene]-3-methyl-isoxazole-5-one): Orange needle crystal, yield 67%, m.p.: 239–241 °C. ^{1}H NMR (DMSO-d_6, 400 MHz) δ (ppm): 2.35 (s, 3H, CH_3), 7.32–7.36 (m, 2H, ArH), 7.60 (s, 1H, –CH=), 8.16–8.21 (m, 2H, ArH,), 9.52 (s, 1H, J = 2.4 Hz, pyrrole-H), 12.81 (s, 1H, NH). ^{13}C NMR (DMSO-d_6, 400 MHz) δ (ppm): 10.7, 108.3, 112.2, 112.7, 118.4, 122.1, 123.5, 127.5, 135.9, 138.0, 140.0, 161.2, 169.9. IR (KBr) υ: 3458 (m. b, υ_{N-H}), 3157, 3125, 3063 (m, $\upsilon_{=C-H}$), 2939 (m, υ_{C-H}), 1701 (s, $\upsilon_{C=O}$), 1599 (s, $\upsilon_{C=C}$), 1582, 1452 (vs, $\upsilon_{C=C}$ $\upsilon_{C=N}$), 1377, 1348, 1298, 1219 ($\upsilon_{C=C}$), 1109, 995 (δ_{CH}), 878 (υ_{N-O}), 812, 756 (m, $\delta_{=CH}$). Anal. Calcd. for $C_{13}H_{10}N_2O_2 = 226.23$: C, 69.02; H, 4.01; N, 12.37; Found: C, 69.42; H, 4.26; N, 12.38. UV–Vis (MeOH) λ_{max}: 426.4 nm.

Dye (**2**) (4-[(5-Benzyloxy-1*H*-indole-3-yl)-methylene]-3-methyl-isoxazole-5-one): Red columnar crystal, yield 60%, m.p.: 240–242 °C. ^{1}H NMR (DMSO-d_6, 400 MHz) δ (ppm): 2.36 (s, 3H, CH_3), 5.19 (s, 2H, CH_2), 7.02 (dd, 1H, J_1 = 2.0 Hz, J_2 = 8.4 Hz, ArH), 7.36 (d, 1H, J = 7.6 Hz, ArH), 7.42 (t, 2H, J_1 = 7.6 Hz, J_2 = 8.4 Hz, ArH), 7.52 (t, 3H, $J_1 = J_2$ = 8.4 Hz, ArH), 7.89 (d, 1H, J = 2.0 Hz, ArH), 8.20 (s, 1H, –CH=), 9.47 (s, 1H, Pyrrole-H), 12.71 (s, 1H, NH). ^{13}C NMR (DMSO-d_6, 400 MHz) δ (ppm): 10.9, 69.6, 102.5, 107.6, 112.4, 113.3, 113.5, 127.4, 128.0, 128.7, 130.8, 136.7, 138.4, 140.0, 154.9, 161.2, 170.1. IR (KBr) υ: 3454 (m. b, υ_{N-H}), 3119, 3094, 3063 (m, $\upsilon_{=C-H}$), 2922 (m, υ_{C-H}), 1703 (s, $\upsilon_{C=O}$), 1595 (s, $\upsilon_{C=C}$), 1580, 1439 (s, $\upsilon_{C=C}$ $\upsilon_{C=N}$), 1375, 1337, 1288, 1200, 1132($\upsilon_{C=C}$), 1107, 990 (δ_{CH}), 874 (υ_{N-O}), 789, 727 (m, $\delta_{=CH}$). Anal. Calcd. for $C_{20}H_{16}N_2O_3 = 332.35$: C, 72.28; H, 4.85; N, 8.43; Found: C, 72.42; H, 4.62; N, 8.39. UV–Vis (MeOH) λ_{max}: 433.6 nm.

2.2. Measurements

The starting materials were commercially available and used as received without additional purification. The solvents used were of analytical grade. Melting points were taken using an XT-4 micro-melting apparatus and were uncorrected. Elemental analyses were performed using a Vario EL-III instrument, while IR spectra, in cm^{-1}, were recorded on a Bruker Equiox-55 spectrometer. ^{1}H NMR and ^{13}C NMR spectra were recorded at 400 MHz using a Varian Inova-400 spectrometer, and chemical shifts were reported relative to the internal Me_4Si. The absorption spectra were recorded on a Shimadzu UV-2450 UV–Vis spectrometer using water, dimethyl sulphoxide, methanol, ethanol and ethyl acetate as solvents, each at a concentration of 10^{-5} M, in 1 cm quartz cells.

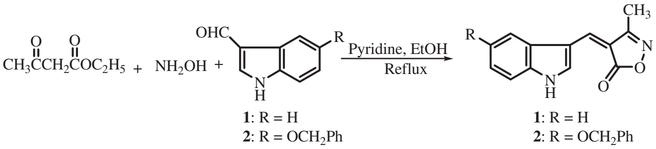

Scheme 1. Synthesis of merocyanine dyes (**1**) and (**2**).

Crystals with approximate dimensions of 0.38 × 0.25 × 0.13 mm^3 for dye (**1**) and 0.31 × 0.26 × 0.13 mm^3 for dye (**2**) were selected for data collection. The X-ray diffraction data were collected using a Bruker SMART APEX II CCD X-ray crystallography system that was equipped with graphite monochromated Mo $K\alpha$ radiation (λ = 0.71073 Å) by using $\omega-2\theta$ scan technique at room temperature. The structures were solved by direct methods and refined using the full-matrix least-squares method on F^2 with anisotropic thermal parameters for all non-hydrogen atoms. Hydrogen atoms were generated geometrically. Crystallographic computing was performed with the SHELXTL [24] and PLATON [25] programs. The crystal data, including details concerning data collection and structure refinement for dyes (**1**) and (**2**), are summarized in Table 1. Parameters in CIF format are available as Electronic Supplementary Information from Cambridge Crystallographic Data Center (CCDC 724598, 729689).

2.3. Computational details

The single molecular structures of dyes (**1**) and (**2**) were optimized at the DFT level using 6-311G** and 6-31G* basis sets. DFT calculations were carried out using a hybrid exchange-correlation functional termed B3LYP, which refers to Becke's three-parameter exchange functional (B3) along with the nonlocal correlation functional of Lee, Yang, and Parr (LYP). The PCM model [26] at the B3LYP/6-311G** level was used to study the solvent polarity effect

Table 1
Crystal data of dyes (**1**) and (**2**).

Identification code	(**1**)	(**2**)
Empirical formula	$C_{13}H_{10}N_2O_2$	$C_{20}H_{16}N_2O_3$
Formula weight	226.23	332.35
Temperature (K)	298 (2) K	298 (2) K
Wavelength (Å)	0.71073	0.71073
Crystal system	Orthorhombic	Monoclinic
Space group	Cmca	$P2_1/n$
Unit cell dimensions (Å)	a = 6.6348 (15)	a = 7.3056 (19)
	b = 19.189 (4)	b = 19.681 (5)
	c = 18.074 (4)	c = 11.445 (3)
	β = 90°	β = 105.063 (4)°
Volume (Å^3)	2301.1 (9)	1589.0 (7)
Z	8	4
Calculated density (g/cm^3)	1.323	1.389
Absorption coefficient (mm^{-1})	0.091	0.095
F (0 0 0)	968	696
Crystal size (mm^3)	0.38 × 0.25 × 0.13	0.31 × 0.26 × 0.13
θ Range for data collection	2.12–25.10	2.07–25.10
Limiting indices h, k, l	−6/7, −22/22, −21/16	−8/5, −23/23, −13/7
Reflections collected/unique/R_{int}	5619/1121/0.0270	6425/2692/0.0338
Completeness to θ = 25.10°	100%	95.4%
Data/restraints/parameters	1121/0/114	2692/0/227
Goodness-of-fit on F^2	1.072	1.083
Final R indices [$I > 2\sigma(I)$]	R_1 = 0.0388, wR_2 = 0.1115	R_1 = 0.0618, wR_2 = 0.1635
R indices (all data)	R_1 = 0.0486, wR_2 = 0.1187	R_1 = 0.0835, wR_2 = 0.1830
Largest diff. peak and hole (e Å^{-3})	0.142 and −0.158	0.437 and −0.230

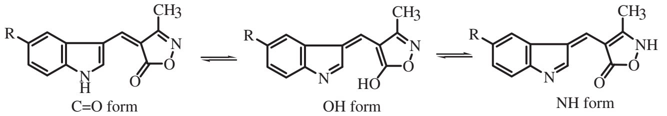

Scheme 2. The equilibrium of three tautomeric forms.

on the absorption spectra. The analytic frequency calculations were performed, and the absence of imaginary frequencies confirmed that the optimized structures were at an energy minimum. The IR spectra were calculated at the B3LYP/6-31G* level, where a modification of the calculated data using the empirical scaling factor 0.9613 [27] was used to achieve better correspondence between the experimental and theoretical values. All calculations reported in this work were performed using the GAUSSIAN 03 program [28].

3. Results and discussion

3.1. Synthesis and characterization

Using a three-component, one-pot method, dyes (**1**) and (**2**) were successfully synthesized and high yields were obtained (60% and 67%, respectively). The products were purified by recrystallization using ethanol or methanol. The choice of the solvent had a crucial effect on single crystal formation. A single solvent (e.g., ethanol, methanol or acetone) could not give suitable single crystals, but a mixture of solvents (EtOH–MeOH or EtOH–acetone) gave suitable crystals. The structures of dyes (**1**) and (**2**) were confirmed by elemental analyses, UV–Vis absorption spectra, IR, ^{1}H NMR and ^{13}C NMR data. In all cases, the IR spectra showed typical aromatic absorption ($\upsilon_{=C-H}$: 3157–3063 cm^{-1}, υ_{C-H}: 2939–2922 cm^{-1}, $\upsilon_{C=C}$: 1599–1595 cm^{-1}, and $\delta_{=CH}$: 812–727 cm^{-1}), resonance conjugated unsaturated stretching modes ($\upsilon_{C=C}$, $\upsilon_{C=N}$, 1582–1132 cm^{-1}), the absorption of an indole ring (υ_{N-H} 3458–3454 cm^{-1}), and classical carbonyl stretching vibration ($\upsilon_{C=O}$, 1703–1701 cm^{-1}). A merocyanine dye with an isoxazolone nucleus could have three tautomers: an OH form, a C=O form or an NH form, as Scheme 2 shows. The IR spectra indicated that the dyes were predominantly in the ketonic form. Moreover, calculations were performed at the B3LYP/6-311G** level for all possible structures of dyes (**1**) and (**2**) in Scheme 2. The single point energies of the C=O, OH and NH forms were −761.512758, −761.4747822 and −761.104039 hartrees for dye (**1**), and −1107.170345, −1107.133618 and −1107.1364861 hartrees for dye (**2**). Obviously, the C=O form was the most stable form of all the potential tautomers, and these results were also consistent with the crystal structure analysis.

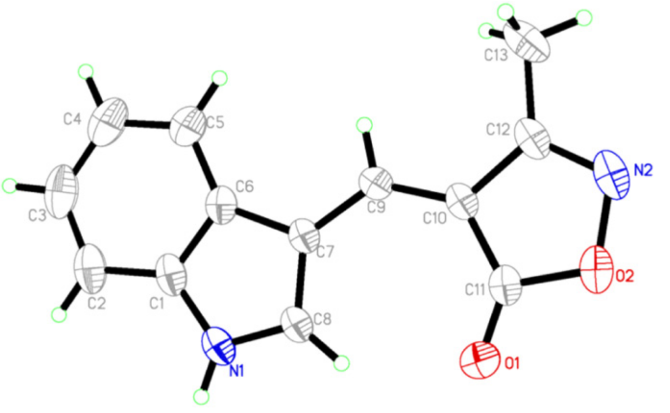

Fig. 1. ORTEP diagram of (**1**) with ellipsoids drawn at the 50% probability level.

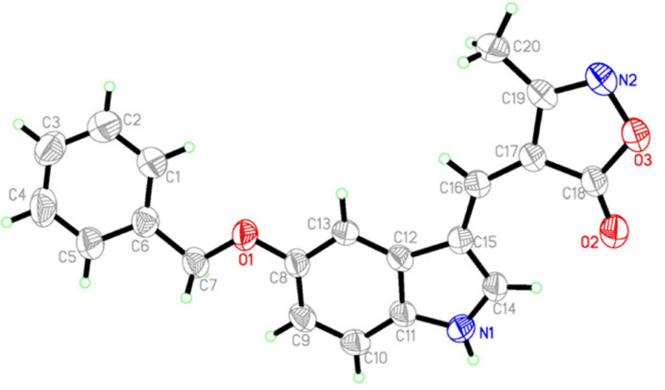

Fig. 2. ORTEP diagram of (**2**) with ellipsoids drawn at the 50% probability level.

3.2. Crystal structure

The molecular structures and atom numbering of (**1**) and (**2**) are shown in Figs. 1 and 2, and the key geometric parameters of dyes (**1**) and (**2**), based on X-ray diffraction and DFT calculations, are presented in Fig. 3.

For dyes (**1**) and (**2**), it was found that the carbon-carbon bond lengths of the molecular skeletons were intermediate between typical C–C single (1.54 Å) and C=C double (1.34 Å) bonds and that the carbon–nitrogen bond lengths were also intermediate between typical C–N single (1.47 Å) and C=N double (1.27 Å) bonds. All bond angles were close to 120° in the benzene rings and

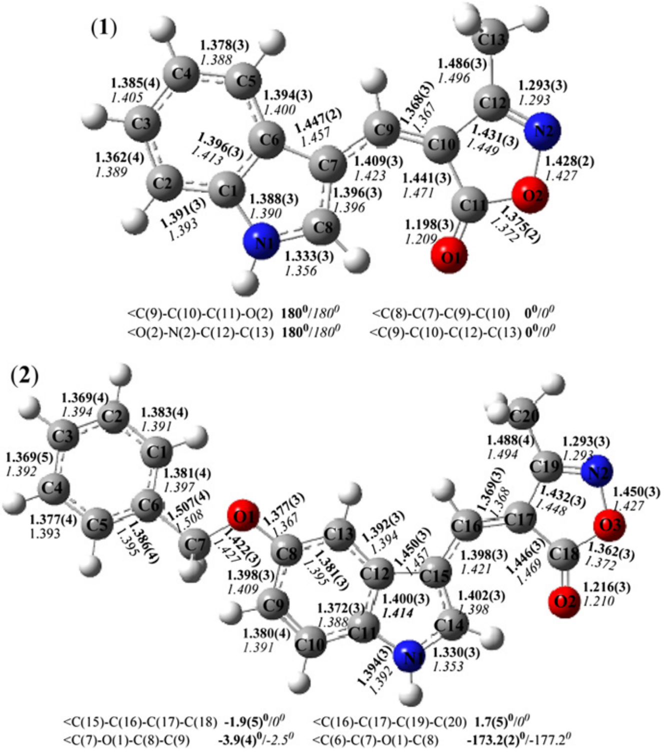

Fig. 3. Selected bond lengths (Å) and torsion angles (°) of dye (**1**) and (**2**) (X-ray diffraction data are in bold type and calculated results by B3LYP/6-311G** are in light italics).

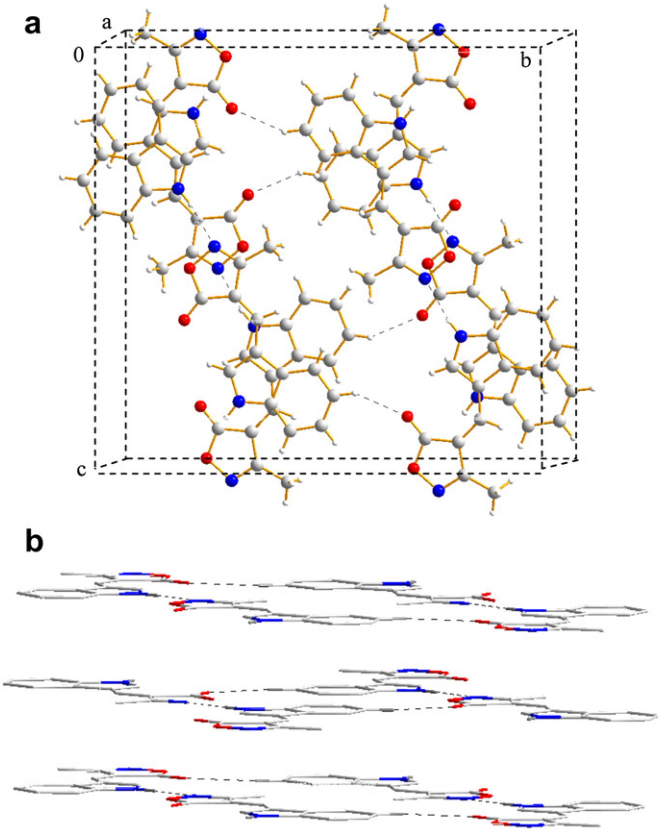

Fig. 4. Crystal packing of (**1**) along the *a* axis (a) and *b* axis (b).

Table 2
The geometry of D–H···A hydrogen bonds of dye (**1**) and (**2**).

Dyes	D–H···A	d(D–H)/Å	D(H···A)/Å	d(D···H)/Å	∠(DHA)/°
(**1**)	N(1)–H(1)···N(2)	0.86	2.04	2.894(2)[a]	171
	C(4)–H(4)···O(1)	0.93	2.46	3.299(3)[b]	150
(**2**)	N(1)–H(1)···O(2)	0.86	1.99	2.842[c]	168

[a] Symmetry code: $-x$, $1/2-y$, $z+1/2$.

[b] Symmetry code: $-x$, $-1/2+y$, $1/2-z$.

[c] Symmetry code: $1/2+x$, $-1/2-y$, $1/2+z$.

close to 108° in the five-membered rings. The π electrons in the whole dye molecule were delocalized, and methyl groups in the isoxazolone rings were involved in the molecular conjugate systems. For dye (**1**), all of the torsion angles were 180° or 0°, which indicates that the molecular framework of (**1**) is planar. For dye (**2**), the C(8)–O(1) (1.377 Å), C(7)–O(1) (1.422 Å) and C(6)–C(7) (1.507 Å) bonds were shorter than conventional C–O single bonds (1.43 Å) or C–C single bonds (1.54 Å), which indicates that the benzyloxy group and the indole ring has *p*–π conjugation. The benzyloxy group was distorted both from planarity and coplanarity within the indole ring, as indicated by the corresponding torsion angles of C(7)–O(1)–C(8)–C(9) and C(6)–C(7)–O(1)–C(8) (−3.9(4)° and −173.2°, respectively). The torsion angles of C(8)–C(7)–C(9)–C(10) (0°) for (**1**) and C(15)–C(16)–C(17)–C(18) (−1.9°) for (**2**) showed that the molecular framework of (**1**) was planar, while the indole and isoxazolone groups were slightly distorted from planarity in (**2**), and this was induced by the benzyloxy group. It could also be seen that the computed bond lengths, bond angles and torsion angles were in good agreement with the experimental data, as shown in Fig. 3. With respect to the experimental values,

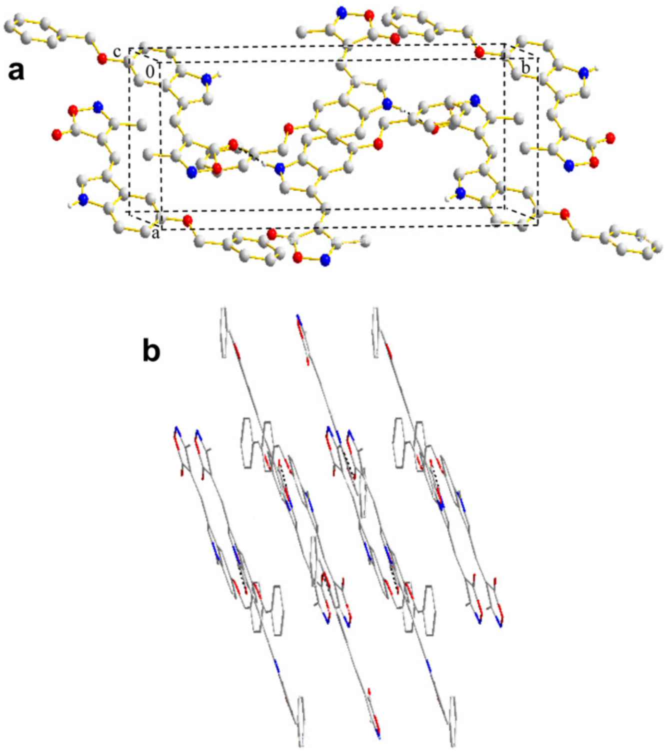

Fig. 5. Crystal packing of (**2**) along the c axis (a) and b axis (b).

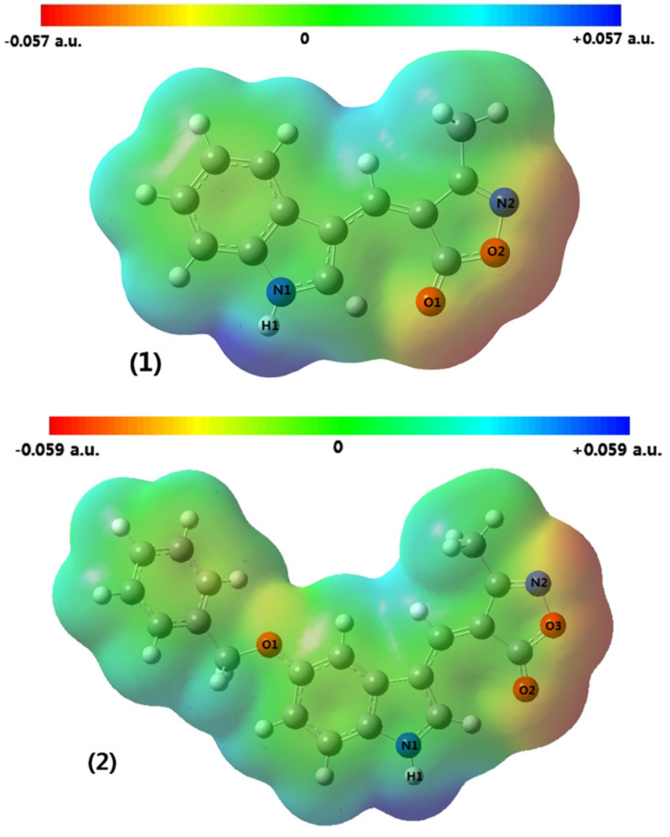

Fig. 6. Molecular electrostatic potential map of (**1**) and (**2**) calculated at the B3LYP/6-311G** level.

Table 3
The physical constants and the spectral data of dyes (**1**) and (**2**) in different solvents.

Solvents	Refractive index/n	Dielectric constant/ε	(**1**)			(**2**)		
			λ_{max}/nm	$\varepsilon \times 10^{-4}$/L mol^{-1} cm^{-1}	$\lambda^{-1} \times 10^3$ (nm^{-1})	λ_{max}/nm	$\varepsilon \times 10^{-4}$/L mol^{-1} cm^{-1}	$\lambda^{-1} \times 10^3$ (nm^{-1})
Ethyl acetate	1.372	6.08	412.2	2.1	2.43	418.4	2.8	2.39
Ethanol	1.361	25.30	426.2	3.1	2.35	433.2	2.8	2.31
Methanol	1.329	33.10	426.4	2.7	2.35	433.6	2.6	2.31
DMSO	1.477	47.24	432.0	2.7	2.31	436.4	2.5	2.29
Water	1.333	80.18	434.0	2.7	2.31	438.8	1.8	2.28

the B3LYP/6-311G** results deviated in the range from 0 Å to 0.027 Å for the bond lengths of (**1**) and from 0 Å to 0.025 Å for the bond lengths and from 1.4° to 4.0° for the torsion angles of (**2**). It appears that the B3LYP/6-311G** method correctly reproduces the signs of the bond lengths, bond angles and torsion angles, which is useful for investigating the characteristics of some structurally-related dyes.

3.3. *Crystal packing and MEP analysis*

The crystal packing of dyes (**1**) and (**2**) along their axes is presented in Figs. 4 and 5. Dyes (**1**) and (**2**) crystallized in the orthorhombic Cmca and monoclinic $P2_1/n$ space groups, respectively. In the packing of (**1**), there were two offset $\pi\cdots\pi$ aromatic, intermolecular interactions that occurred between the pyrrole rings and isoxazolone rings [$Cg1\cdots Cg1 = 3.565(9)$ Å, symmetry code: $-1/2+x, 1/2-y, -z$; $Cg2\cdots Cg2 = 3.489(8)$ Å, symmetry code: $-1/2-x, y, 1/2-z$]. The molecule also contained hydrogen bond acceptor and donor sites, and thus, the classical strong hydrogen bonds N(1)–H(1)···N(2) [symmetry code: $-x, 1/2-y, z+1/2$] and weak hydrogen bonds C(4)–H(4)···O(1) [symmetry code: $-x, -1/2+y, 1/2-z$] existed between molecules (Table 2), which also played crucial roles in the crystal packing. Two types of hydrogen bonds linked neighbouring molecules, in head-to-tail fashion, leading to the formation of hydrogen-bonded chains along the *c* and *b* axes, respectively. However, adjacent molecules of (**2**) were not stacked through classical $\pi\cdots\pi$ interactions, due to steric hindrance from the benzyloxy group, which distorted the molecular planarity. Two types of weak C–H···π intermolecular interactions existed in (**2**), C(7)–H(7B)···π (in the isoxazolone ring) [$C\cdots\pi = 3.721$ Å, symmetry code: $2-x, -y, 1-z$] and C(20)–H(20B)···π (in the benzene ring of indole) [$C\cdots\pi = 3.517$ Å, symmetry code: $1-x, -y, 1-z$]. It was also found that N(1)–H(1)···O(2) hydrogen bonds linked the molecules, forming parallel, infinite sheets along the *b* axis. The strong N–H···O interaction between H(1) and O(2) was found to have a distance of 1.99 Å (Table 2), which was effective in stabilizing the crystal structure.

The molecular electrostatic potential (MEP) was investigated using B3LYP/6-311G**-optimized geometries, as shown in Fig. 6. This method gives information about the proper region by which compounds have intermolecular interactions between their units. In MEP analysis, the negative (red and yellow) and the positive (blue) regions correspond to nucleophilic and electrophilic centers, respectively. The positive (blue) regions of dyes (**1**) and (**2**) were localized on H1 and had electrophilic reactivity. Conversely, the negative (red and yellow) regions were observed at the isoxazolone ring around O1, O2 and N2 for (**1**) and around O2, O3 and N2 for (2) and had nucleophilic reactivity. Hence, the MEP maps clearly showed that the intermolecular hydrogen bonds in the crystal structures were between the positive and negative regions, indicating possible sites for intermolecular interactions.

3.4. *The UV–Vis spectra and the dominant electronic excitations of dyes*

The absorption spectral data of dyes (**1**) and (**2**) in different solvents are listed in Table 3, and a sample UV–Vis spectrum (dye (**1**)) is shown in Fig. 7. All concentrations followed Beer's law, and no changes in the shape of the absorption spectra were observed. Dyes (**1**) and (**2**) absorbed in the range of 412–439 nm and had molar extinction coefficients of 1.8×10^4–3.1×10^4 L mol^{-1} cm^{-1}. The electronic absorption spectra of the dyes in different solvents exhibited an intense absorption with high extinction coefficients,

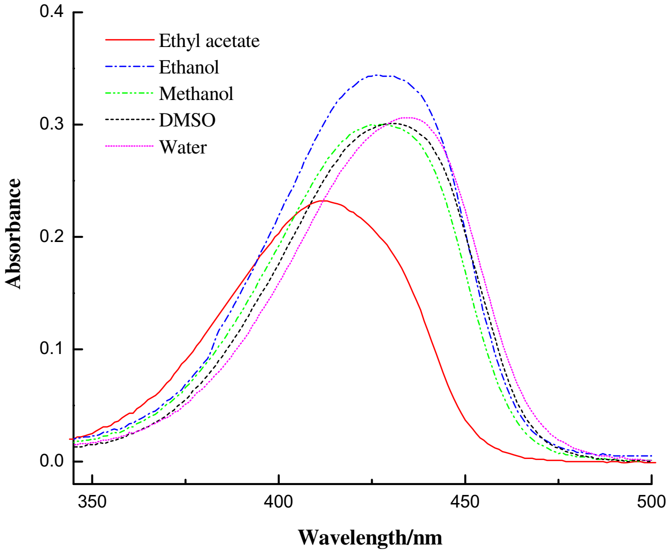

Fig. 7. UV–Vis absorption spectra of (**1**) in different solvents.

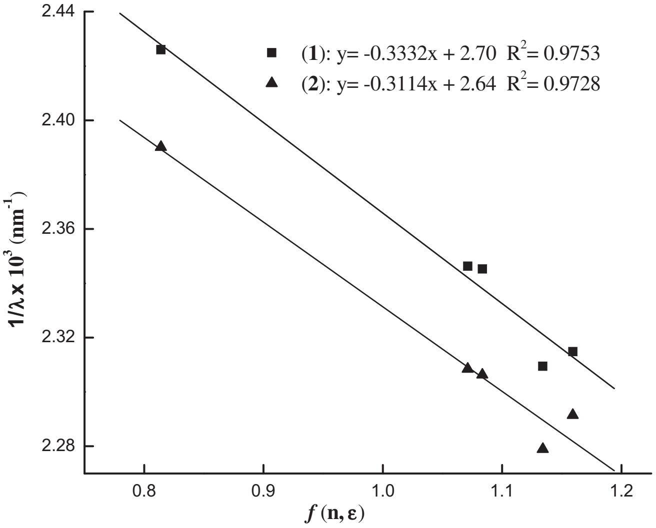

Fig. 8. Correlation of wavenumbers ($1/\lambda$) in various solvents vs. $f(n, \varepsilon)$ of dyes (**1**) and (**2**).

Table 4
Main calculated orbital transitions.

Dyes	Excited state	Gas/TD-B3LYP			Methanol/TD-B3LYP (PCM)			ΔE/ev
		ΔE/ev	f[a]	Transition character[b]	ΔE/ev	f[a]	Transition character[b]	
(**1**)	1	3.4210	0.4421	HOMO → LUMO (98.24%)	3.2803	0.5175	HOMO → LUMO (98.56%)	2.9077
	2	3.6527	0.0003	HOMO-3 → LUMO (98.64%)	3.6199	0.0324	HOMO-1 → LUMO (98.08%)	
	3	3.7969	0.0291	HOMO-1 → LUMO (95.95%)	3.8923	0.0003	HOMO-3 → LUMO (98.61%)	
(**2**)	1	3.2065	0.3086	HOMO → LUMO (76.21%)	3.0193	0.3112	HOMO → LUMO (83.46%)	2.8564
	2	3.5453	0.2018	HOMO-1 → LUMO (73.68%)	3.3953	0.2725	HOMO-1 → LUMO (81.21%)	
	3	3.6665	0.0003	HOMO-4 → LUMO (98.52%)	3.9086	0.0003	HOMO-5 → LUMO (98.62%)	

[a] Oscillator strength.
[b] The proportion of the main transition is given in parentheses.

due to π–π* electronic transitions. The $\lambda_{\max}$ of dye (**2**) was 4.4–7.2 nm greater than that of dye (**1**), which was due to increased conjugation in the dyes. It was also found that the absorption maxima showed a clear red shift when passing from the low-polar solvents to the high-polar solvents. It is suggested that dyes with π–π* transitions are more polar in their excited states than in their ground states. In another study, a spectral red shift in high-polar solvents was concluded to be mainly due to a greater degree of energy reduction of the excited states than that of ground states [29]. As a preliminary study of the solute–solvent interactions, the Bayliss function $[f\ (n,\ \varepsilon) = (n^2 - 1)/(2n^2 + 1) + (\varepsilon - 1)/(\varepsilon + 2)]$ was used, where n was the refractive index and ε was the static dielectric constant of the solvents. Calculated f values ranged from 0.811, for ethyl acetate, to 1.156, for DMSO. Plotting the results of $1/\lambda$ with $f(n, \varepsilon)$ is shown in Fig. 8, and the correlation between $1/\lambda$ and $f\ (n,\ \varepsilon)$ provided an adjusted R^2 value of 0.97. This function indicated that the spectral shifts were essentially due to dispersion, induced electronic polarization and an induced dipole moment. However, a limitation of the function is that it does not include intermolecular interactions and hydrogen-bonding interactions, and this is the main reason for deviation of the linear correlation.

The experimental excitation energies, calculated main orbital compositions of the computed lower-lying singlet excited states, transition features and oscillator strengths (f) of the dyes are given in Table 4. The TDDFT calculations predicted three transition states and only one dominant transition by the largest oscillator strength for the dyes. The lowest energy absorption of the dyes corresponded to the first dipole-allowed π–π* electronic transition from HOMO to LUMO orbitals, which could be attributed to intramolecular charge transfer (ICT) in the dyes. The sketches of the molecular orbitals (MOs) for dyes (**1**) and (**2**) are illustrated in Fig. 9. Nearly all of the MOs in the HOMO of (**1**) and (**2**) were substantially localized on the indole and isoxazolone rings, and only a few contributions from the OCH_2 fragment for (**2**) were observed. The MOs in the LUMO were mainly distributed at the pyrrole ring, isoxazolone nucleus and methylidyne fragments. The excitation involved the intramolecular electron displacement from the indole groups to the isoxazolone moiety, whereas indole and isoxazolone groups acted as electron donors and electron acceptors, respectively. The HOMO and LUMO energy values were −6.7561 eV and −2.5288 eV for (**1**), and −5.90873 eV and −2.4891 eV for (**2**), respectively, at the DFT level, and the calculated energy gaps were 4.23 eV and 3.42 eV for (**1**) and (**2**), respectively. Dye (**2**), which has a smaller frontier orbital gap, was more polarizable than dye (**1**) [30].

3.5. IR spectra

Since IR spectra can give important information on the identification of compounds, the vibrational analysis of dyes (**1**) and (**2**) was also performed at both the experimental and theoretical calculation B3LYP/6-31G* levels. For comparison, the observed and simulated IR spectra are presented in Fig. 10. From the theoretical

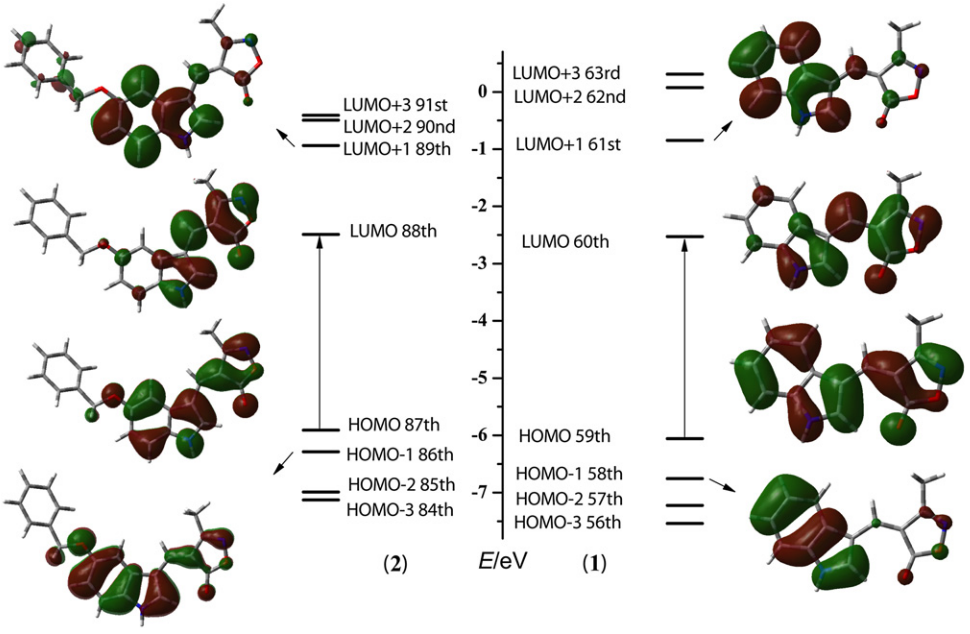

Fig. 9. Molecular orbitals of dyes (**1**) (right) and (**2**) (left).

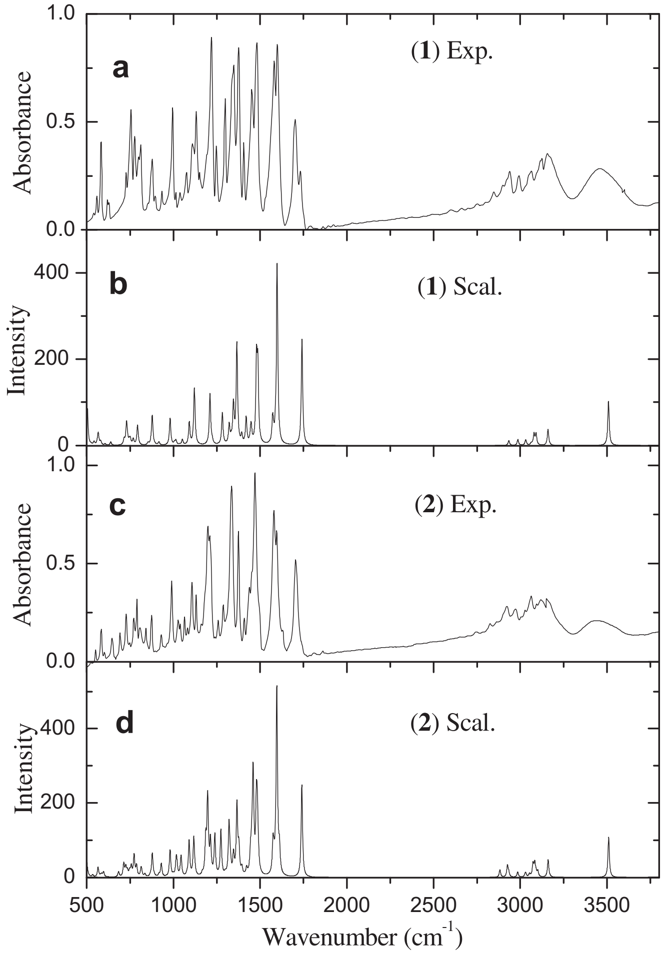

Fig. 10. The experimental IR spectra (a: (**1**); c: (**2**)) and scaled simulated IR spectra at the B3LYP/6-31G* level (b: (**1**); d: (**2**)).

calculations, $3n - 6$ frequencies (75 and 117 frequencies for dyes (**1**) and (**2**), respectively) were found. However, the intensities of the majority of the frequencies were low; therefore, the typical frequencies are reported in Table 5. The calculated spectra were found to be higher than the experimental values, possibly because the electron correlation and vibrational anharmonicity were neglected by this calculation. For reducing the systematic errors, the scaling factor 0.9613 [27] was used for the calculated harmonic vibrational wavenumbers at the B3LYP/6-31G* level. The adjusted R^2 values were 0.9997 and 0.9996 for dyes (**1**) and (**2**), which indicated good linearity between the scaled and experimental wavenumbers, as shown in Fig. 11.

Based on the good agreement between the scaled and observed IR spectra and the structural similarity between dyes (**1**) and (**2**), further studies on the assignment of the dyes were carried out. In Fig. 10 and Table 5, it is shown that the typical vibrations of (**1**) were very similar to that of (**2**). However, the wavenumbers of (**1**) were slightly higher than that of (**2**), and this could be because of the lower energy of (**2**) in a larger conjugated system, as was discussed in section 3.1. Obviously, the experimental vibrational frequencies at 3458 cm^{-1} and 3454 cm^{-1} for dye (**1**) and (**2**), respectively, were classified as the mode 1# $\upsilon_{\mathrm{N-H}}$, and the frequencies at 3157 cm^{-1} for (**1**) and at 3119 cm^{-1} for (**2**) were classified as the mode 2# C–H stretching vibrations of the pyrrole rings. Two C–H stretching vibrations were detected in the benzene rings, with wavenumbers falling in the region of 3063–3125 cm^{-1}. The C–H stretching vibrations of the methyl and methylene groups (mode 5#) were detected at lower wavenumbers (2939–22 922 cm^{-1}), in comparison to the aromatic C–H stretching modes. The strong bands at about 1700 cm^{-1} were attributed to the C=O stretching vibrational mode. The dyes within whole, molecular conjugate systems were predicted to have significant C–C and C–N bond stretching modes ranging from 1598 to 1117 cm^{-1}, which was in excellent agreement with the experimental observation ranging from 1132 to 1599 cm^{-1}. The normal vibration 16, 17, and 19# modes and the 20# mode were classified as C–H in-plane bending and out-of-plane vibrations in the range of 1109–789 cm^{-1} and 756–727 cm^{-1}, respectively. There were also medium bands (mode 18#) ranging from 874 to 878 cm^{-1}, and these were referred to as N–O stretching vibration.

Table 5
The measured IR, calculated vibrational wavenumbers at the B3LYP/6-31G* level and assignments for dyes (**1**) and (**2**).

Mode	Vibratory feature	(**1**)				(**2**)			
		Exp.[a]	Cal.	Scal.[b]	Int.	Exp.[a]	Cal.	Scal.[b]	Int.
1#	$\upsilon_{\mathrm{N-H}}$ (pyrrole)	3458 (m)	3650	3508	102.74	3454 (m)	3651	3509	108.40
2#	$\upsilon_{\mathrm{=C-H}}$ (pyrrole)	3157 (m)	3287	3160	37.47	3119 (m)	3288	3161	47.77
3#	$\upsilon_{\mathrm{=C-H}}$ (benzene)	3125 (w)	3215	3091	25.74	3094 (m)	3207	3083	34.63
4#	$\upsilon_{\mathrm{=C-H}}$ (benzene)	3063 (w)	3203	3079	25.55	3063 (m)	3196	3073	23.58
5#	$\upsilon_{\mathrm{C-H}}$ (CH_3, CH_2)	2939 (m)	3052	2934	11.06	2922 (m)	3044	2926	30.89
6#	$\upsilon_{\mathrm{C=O}}$	1701 (s)	1811	1741	246.03	1703 (s)	1810	1740	248.54
7#	$\upsilon_{\mathrm{C=C}}$	1599 (vs)	1662	1598	419.27	1595 (s)	1660	1596	501.95
8#	$\upsilon_{\mathrm{C=C}}$, $\upsilon_{\mathrm{C=N}}$	1582 (vs)	1635	1572	54.13	1580 (vs)	1638	1574	78.83
9#	$\upsilon_{\mathrm{C=C}}$, $\upsilon_{\mathrm{C=N}}$	1481 (s)	1547	1487	167.21	1472 (w)	1538	1479	170.01
10#	$\upsilon_{\mathrm{C=C}}$, $\upsilon_{\mathrm{C=N}}$	1452 (vs)	1539	1479	181.28	1439 (s)	1517	1458	182.82
11#	$\upsilon_{\mathrm{C=C}}$, $\upsilon_{\mathrm{C=N}}$	1377 (s)	1421	1366	233.48	1375 (vs)	1421	1366	189.21
12#	$\upsilon_{\mathrm{C=C}}$	1348 (m)	1400	1346	90.41	1337 (w)	1374	1321	136.69
13#	$\upsilon_{\mathrm{C=C}}$	1298 (vs)	1334	1282	73.80	1288 (s)	1325	1274	122.97
14#	$\upsilon_{\mathrm{C=C}}$, $\upsilon_{\mathrm{C=N}}$	1219 (m)	1259	1211	119.05	1200 (m)	1246	1197	208.29
15#	$\upsilon_{\mathrm{C=C}}$	1132 (w)	1166	1121	125.50	1132 (m)	1162	1117	103.67
16#	δ_{CH}	1109 (m)	1135	1091	52.09	1107 (m)	1134	1090	95.98
17#	δ_{CH}	995 (m)	1020	981	62.14	990 (m)	1020	981	68.48
18#	$\upsilon_{\mathrm{N-O}}$	878 (m)	914	878	67.46	874 (w)	914	879	63.42
19#	$\delta_{\mathrm{=CH}}$	812 (m)	825	793	45.84	789 (m)	804	773	57.97
20#	$\delta_{\mathrm{=CH}}$	756 (m)	759	730	50.25	727 (m)	755	725	25.29

[a] vs: very strong, s: strong, m: middle, w: weak for IR intensity.
[b] The scaling factor 0.9613 was used for the wavenumbers obtained at the B3LYP/6-31G* level.

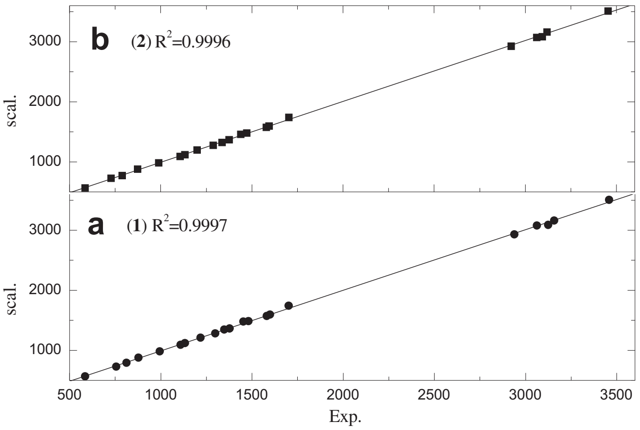

Fig. 11. Graphic correlation between the experimental and the scaled theoretical frequencies obtained by the B3LYP/6-31G* level (a: (**1**); b: (**2**)).

4. Conclusion

The results of X-ray and theoretical calculation analyses indicated that merocyanine dyes containing an isoxazolone nucleus prefer to be in the ketonic form when in a solid state. Dyes (**1**) and (**2**) crystallized in the orthorhombic Cmca space group and monoclinic $P2_1/n$ space group, respectively. In dye (**1**), intermolecular N(1)–H(1)···N(2) and C(4)–H(4)···O(1) hydrogen bonds and offset $\pi\cdots\pi$ aromatic interactions stabilized the crystal structure. In dye (**2**), there were two types of weak C–H···π intermolecular interactions that existed, and N(1)–H(1)···O(2) hydrogen bonds linked the molecules into parallel, infinite sheets along the *b* axis. The molecular electrostatic potential (MEP) obtained by B3LYP/6-311G** clearly showed the possible sites for nucleophilic attack among the crystal packing. Using the scaling factor 0.9613 to remove the major systematic errors of B3LYP/6-31G*, the IR spectra could be predicted with high accuracy.

Acknowledgements

We appreciate the financial support for this research by the Program of the National Basic Research and Development Program of China (973) under Grant No. 2011CB707702; the National Natural Science Foundation of China under Grant Nos. 81090272, 81000632, 30900334, 81101083, 81101084, 81101100; the Shaanxi Provincial Natural Science Foundation Research Project under Grant No. 2009JQ8018, and the Science Research Startup Foundation of Xidian University (K50510100002, K50510100004, K50510100005).

References

[1] Deng B-L, Hartman TL, Robert W, Buckheit J, Pannecouque C, Clercq ED, et al. Replacement of the metabolically labile methyl esters in the alkenyldiarylmethane series of non-nucleoside reverse transcriptase inhibitors with isoxazolone, soxazole, oxazolone, or cyano substituents. J Med Chem 2006;49:5316–23.
[2] Ishioka T, Kubo A, Koiso Y, Nagasawa K, Itaib A, Hashimoto Y. Novel nonsteroidal/non-anilide type androgen antagonists with an isoxazolone moiety. Bioorg Med Chem 2002;10:1555–66.
[3] Ishioka T, Tanatani A, Nagasawa K, Hashimoto Y. Anti-androgens with full antagonistic activity toward human prostate tumor LNCaP cells with mutated androgen receptor. Bioorg Med Chem Lett 2003;13:2655–8.
[4] Laughlin SK, Clark MP, Djung JF, Golebiowski A, Brugel TA, Sabat M, et al. The development of new isoxazolone based inhibitors of tumor necrosis factor-alpha (TNF-α) production. Bioorg Med Chem Lett 2005;15:2399–403.
[5] Lowe DB, Magnuson S, Qi N, Campbell A-M, Cook J, Hong Z, et al. In vitro SAR of (5-(2H)-isoxazolonyl) ureas, potent inhibitors of hormone-sensitive lipase. Bioorg Med Chem Lett 2004;14:3155–9.
[6] Dayan FE, Duke SO, Reddy KN, Hamper BC, Leschinsky KL. Effects of isoxazole herbicides on protoporphyrinogen oxidase and porphyrin physiology. J Agric Food Chem 1997;45(3):967–75.
[7] Hess FD. Light-dependent herbicides: an overview. Weed Sci 2000;48(2):160–70.
[8] Aret E, Meekes H, Vlieg E, Deroover G. Polymorphic behavior of a yellow isoxazolone dye. Dyes Pigments 2007;72:339–44.
[9] Deij MA, Horst JHt, Meekes H, Jansens P, Vlieg E. Polymorph formation studied by 3D nucleation simulations. Application to a yellow isoxazolone dye, paracetamol, and L-glutamic acid. J Phys Chem B 2007;111:1523–30.
[10] Alías S, Andreu R, Blesa MJ, Cerdán MA, Franco S, Garín J, et al. Iminium salts of ω-dithiafulvenylpolyenals: an easy entry to the corresponding aldehydes and doubly proaromatic nonlinear optic-phores. J Org Chem 2008;73:5890–8.
[11] Lee J-E, Kim HJ, Han MR, Lee SY, Jo WJ, Lee SS, et al. Crystal structures of C.I. disperse red 65 and C.I. disperse red 73. Dyes Pigments 2009;80:181–6.
[12] Laufer SA, Margutti S. Isoxazolone based inhibitors of p38 MAP kinases. J Med Chem 2008;51(8):2580–4.
[13] Kim K-H, Jung DH, Kim D, Lee A, Choi K, Kim Y, et al. Crystal structure prediction of organic materials: tests on the 1,4-diketo-3,6-diphenylpyrrolo(3,4-c)pyrrole and 1,4-diketo-3,6-bis(4′- dipyridyl)-pyrrolo-[3,4-c]pyrrole. Dyes Pigments 2011;89:37–43.
[14] Ebead YH. Spectrophotometric investigations and computational calculations of prototropic tautomerism and acid-base properties of some new azo dyes. Dyes Pigments 2011;92(1):705–13.
[15] Kim S, Mor GK, Paulose M, Varghese OK, Baik C, Grimes CA. Molecular design of near-IR harvesting unsymmetrical squaraine dyes. Langmuir 2010;26(16):13486–92.
[16] Kolev T, Tsanev T, Kotov S, Mayer-Figge H, Spiteller M, Sheldrick WS, et al. Anyles of 4-benzoylpyridine – crystal structure and spectroscopic properties. Dyes Pigments 2009;82:95–101.
[17] Casanova D, Rotzinger FP, Grätzel M. Computational study of promising organic dyes for high-performance sensitized solar cells. J Chem Theory Comput 2010;6(4):1219–27.
[18] Preat J. Photoinduced energy-transfer and electron-transfer processes in dye-sensitized solar cells: TDDFT insights for triphenylamine dyes. J Phys Chem C 2010;114(39):16716–25.
[19] Meguellatia K, Ladamea S, Spichty M. A conceptually improved TD-DFT approach for predicting the maximum absorption wavelength of cyanine dyes. Dyes Pigments 2011;90(2):114–8.
[20] Fu YL, Huang W, Li CL, Wang LY, Wei YS, Huang Y, et al. Monomethine cyanine dyes with an indole nucleus: microwave-assisted solvent-free synthesis, spectral properties and theoretical studies. Dyes Pigments 2009;82:409–15.
[21] Sajan D, Vijayan N, Safakath K, Philip R, Joe IH. Intramolecular charge transfer and Z-Scan studies of a semiorganic nonlinear optical material sodium acid phthalate hemihydrate: a vibrational spectroscopic study. J Phys Chem A 2011;115(29):8216–26.
[22] Rieff B, Bauer S, Mathias G, Tavan P. IR spectra of flavins in solution: DFT/MM description of redox effects. J Phys Chem B 2011;115(9):2117–23.
[23] Zhang YQ, Ma JJ, Wang C, Li JC, Zhang DN, Zang XH, et al. One-pot synthesis of 3-methyl-4-arylmethylene-isoxazol-5(4H)-ones. Chin J Org Chem 2008;28:141–4.
[24] Bruker. SHELXTL, version 5.1. Madison, WI: Bruker AXS Inc.; 1999.
[25] Spek AL. Structure validation in chemical crystallography. Acta Crystallogr 2009;D65:148–55.
[26] Tomasi J, Mennucci B, Cammi R. Quantum mechanical continuum solvation models. Chem Rev 2005;105:2999–3093.
[27] Scott AP, Radom L. Harmonic vibrational frequencies: an evaluation of Hartree-Fock, Møller-Plesset, quadratic configuration interaction, density functional theory, and semiempirical scale factors. J Phys Chem 1996;100:16502–13.
[28] Frisch MJ, Trucks GW, Schlegel HB, Scuseria GE, Robb MA, Cheeseman JR, et al. Gaussian 03. Revision B.03. Pittsburgh PA: Gaussian, Inc.; 2003.
[29] Airinei A, Homocianu M, Dorohoi DO. Changes induced by solvent polarity in electronic absorption spectra of some azo disperse dyes. J Mol Liq 2010;157:13–7.
[30] Powell BJ, Baruah T, Bernstein N, Brake K, McKenzie RH, Meredith P, et al. A first-principles density-functional calculation of the electronic and vibrational structure of the key melanin monomers. J Chem Phys 2004;120(18):8608–15.